Polynomial Description of the Fe–C–Si Stable Phase Diagram for up to 4.5 wt% Si, Including the Effect of Cr, Cu, Mn and P

Jon Sertucha, Jacques Lacaze, Anna Regordosa, Ramon Suarez

POLYNOMIAL DESCRIPTION OF THE Fe–C–Si STABLE PHASE DIAGRAM FOR UP TO 4.5 WT% Si, INCLUDING THE EFFECT OF Cr, Cu, Mn AND P

Jon Sertucha, Anna Regordosa and Ramon Suarez
Azterlan, Basque Research and Technology Alliance, Aliendalde 6, 48200 Durango, Bizkaia, Spain

Jacques Lacaze
CIRIMAT, Université de Toulouse, 4 allée Monso, BP 44362, 31030 Toulouse, France

https://doi.org/10.1007/s40962-024-01428-z

Abstract

Knowledge of the relevant stable equilibrium phase diagram is a prerequisite for taking account of deviations from equilibrium when modeling the solidification of silicon cast irons. While a linear description is practical for silicon contents up to 3 wt%, the curvature of the austenite liquidus at higher silicon contents necessitates the use of second-order polynomials. This study was carried out with the aim of obtaining an accurate description up to 4.5 wt% silicon, representative of today's emerging high-silicon cast irons. In addition, alloying with up to 1 wt% copper, 0.5 wt% manganese and 0.25 wt% chromium and phosphorus was considered. In parallel to a description of the liquidus of austenite and graphite, the austenite-liquid partition coefficients of all alloying elements have been described. This paves the way for future work aimed at providing an accurate description of microsegregation and other non-equilibrium phenomena occurring during the solidification of silicon cast irons.

Keywords: *solidification, cast irons, Fe–C–Si phase diagram, alloying elements, partition coefficients*

Introduction

The carbon equivalent liquidus (CEL) of austenite and the eutectic carbon equivalent (CE) are of common use for process control of silicon cast irons. For usual cast irons with nominal silicon content less than 3 wt%, these quantities have often been expressed as linear relations of carbon and silicon contents, with sometimes account made to other elements such as phosphorus, copper, etc. These linear relationships have been shown to be directly associated with a linear description of the austenite and graphite liquidus of the equilibrium Fe–C–Si system[1,2] that is adequate when the silicon content is limited to 3 wt%. Accounting for the kinetic effects in the nucleation and growth processes involved in the solidification of cast irons straightforwardly explains the systematic shift between equilibrium phase diagram and recorded liquidus and eutectic temperatures. This has been detailed in successive works[3–6] where a discussion of the relevant literature[7–18] can be found.

With the development of high silicon cast irons, there is a need for a similar polynomial description of the relevant equilibrium phase diagram up 4.5 wt%. However, the austenite liquidus curves at silicon contents higher than 3 wt%, cannot be anymore linearly described. This was the aim of this work to derive as simple as possible appropriate polynomials valid up to 4.5 wt% silicon, and this was achieved based on the equilibrium phase diagram calculated with the TCFE-8 database of ThermoCalc.[19] A similar procedure limited to low silicon content and a linear description of CE has already been used by Bazhenov and Pikunov.[20] In the present work, the effect of other elements, copper up to 1 wt%, manganese up to 0.5 wt%, and chromium and phosphorus up to 0.25 wt%, was also considered, and the partition coefficient between austenite and liquid of all alloying elements including carbon was described. The following section presents the Fe–C–Si ternary phase diagram and the next section the effect of the four additional elements.

Received: 12 June 2024 / Accepted: 28 July 2024
Published online: 15 August 2024

Ternary Fe-C-Si System

Isopleth sections were calculated with TCFE-8 for four different silicon contents (0, 2, 3 and 4.5 wt%) and are plotted with dotted lines in Figure 1: the austenite liquidus, T_L^{γ}, decreases with carbon content, while the graphite liquidus, T_L^{gra}, raises with it (all temperatures will be expressed in Celsius). The intersection of the two liquidus at given silicon content defines the corresponding eutectic point. At temperature below this point, the liquidus lines are metastable extensions that are of interest as solidification of cast irons proceeds with some undercooling.

Each of the lines calculated with TCFE-8 could be fitted as a linear relation of the carbon content with a regression coefficient virtually equal to 1. These relations are defined as:

$$T_L^{\gamma} = T_0^{\gamma} + m_C^{\gamma} \cdot w_C \qquad \text{Eqn. 1}$$

for austenite, and

$$T_L^{gra} = T_0^{gra} + m_C^{gra} \cdot w_C \qquad \text{Eqn. 2}$$

for graphite.

In the above expressions T_0^{γ} and T_0^{gra} are appropriate constants, m_C^{γ} and m_C^{gra} stand for the liquidus slope of austenite and graphite liquidus, respectively, and w_C is the alloy carbon content (wt%). All four coefficients depend on the alloy silicon content, w_{Si} (wt%), and could be expressed as second order polynomials of it:

$$T_0^{\gamma} = 1639.0 - 49.652 \cdot w_{Si} + 2.7506 \cdot (w_{Si})^2 \qquad \text{Eqn. 3}$$

$$m_C^{\gamma} = -112.21 + 6.0457 \cdot w_{Si} - 0.51415 \cdot (w_{Si})^2 \qquad \text{Eqn. 4}$$

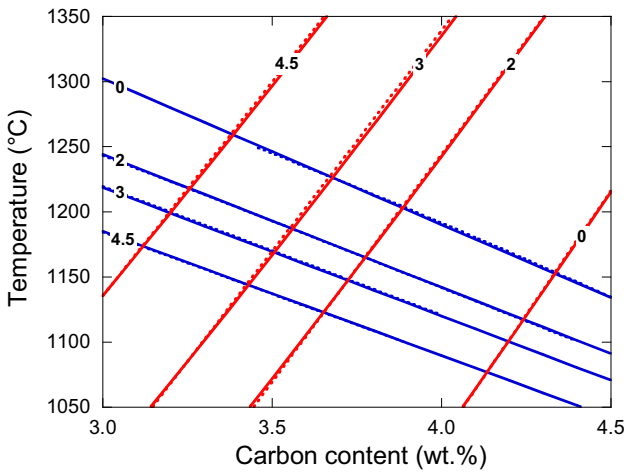

Figure 1. Isopleth diagram of the austenite and graphite liquidus. The dotted lines have been calculated with TCFE-8 and the solid lines are obtained from the polynomial Eqns. (1) and (2) with the appropriate parameters expressed in Eqns. (3–6). Numbers indicate the silicon content.

$$T_0^{gra} = -503.34 + 196.46 \cdot w_{Si} - 11.368 \cdot (w_{Si})^2 \qquad \text{Eqn. 5}$$

$$m_C^{gra} = 382.24 - 19.408 \cdot w_{Si} + 1.6522 \cdot (w_{Si})^2 \qquad \text{Eqn. 6}$$

Equations (3–6) have been introduced in Eqns. (1) and (2) and plotted with solid lines in Figure 1. It is considered an excellent, if not perfect, agreement between these linear relations and the calculations using TCFE-8 that demonstrates Eqns. (3–6) are valid up to 4.5 wt% Si. The adjustment was made to approximate the liquidus of austenite and graphite around the eutectic point, meaning that calculations were made from 3 to 4.5 wt% C for 0 wt% Si, and 2.5 to 4.5 wt% C for 4.5 wt% Si. These intervals define the compositional range where Eqns. (1) and (2) can be applied with the parameters listed in Eqns. (3–6).

By equating the austenite and graphite liquidus temperatures expressed with Eqns. (1) and (2), one gets an expression that relates the carbon and silicon contents along the eutectic line. The eutectic carbon content, w_C^{eut}, is thus (wt%):

$$w_C^{eut} = 4.333 \cdot \frac{1 - 0.1149 \cdot w_{Si} + 0.0066 \cdot (w_{Si})^2}{1 - 0.0515 \cdot w_{Si} + 0.0044 \cdot (w_{Si})^2} \qquad \text{Eqn. 7}$$

In Figure 2a, this relation is compared to the TCFE-8 calculation and shows a perfect agreement. On this figure is also shown the linear relation valid up to 3 wt% Si that was given as:[1,4]

$$w_C^{eut} = 4.34 - 0.28 \cdot w_{Si} \qquad \text{Eqn. 8}$$

It is seen that the linear relation previously used (Eqn. 8) slightly deviates from the present evaluation only for silicon contents higher than 3.5 wt%. Note also that the reference value for eutectic carbon equivalent is 4.333 wt% in Eqn. (7) instead of 4.34 wt% in Eqn. (8), while the value calculated with TCFE-8 is 4.338 wt%.

By inserting Eqn. (7) in Eqn. (1) (or Eqn. 2) with the appropriate coefficients (Eqns. 3 and 4 for austenite, or Eqns. 5 and 6 for graphite), one gets the temperature along the eutectic line that is depicted in Figure 2b where it is compared with the temperature evolution calculated directly with TCFE-8. The difference between these curves is at most 1.5°C at 4.5 wt% Si. Also, it is seen that this quadratic description of the phase diagram reproduces very satisfactorily the experimental eutectic temperatures determined by differential thermal analysis that had been used in a previous thermodynamic assessment of the Fe–C–Si system.[21] In contrast, the linear relation that was previously derived[1,4] is also plotted up to 3 wt% Si and is seen to slightly deviate with increase of the silicon content.

Of further interest in the above analysis is the straight definition of the CE value that allows positioning of an

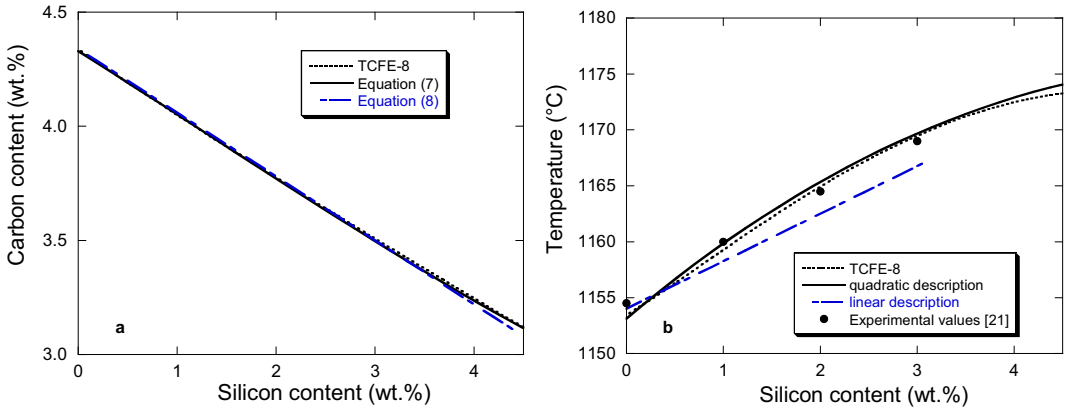

Figure 2. (a) Change in carbon and silicon contents along the eutectic line of the stable Fe–C–Si system. (b) Change of temperature along the eutectic line of the stable equilibrium Fe–C–Si system.

alloy with respect to the eutectic composition. As for the previous linear analysis, Eqn. (8) leads immediately to:

$$CE = w_C + 0.28 \cdot w_{Si} \qquad \text{Eqn. 9}$$

As noticed above, the reference value for the stable equilibrium eutectic is CE = 4.34 wt%. It has been described previously why this value differs from other selected values, and in particular the value of 4.26 wt% that is often used (for literature review and details see References 3–6 and 22).

To get a simple expression of w_C^{eut}, Eqn. (7) could be extended as a Taylor series but a simpler way of doing was carried out here consisting in fitting the carbon content along the eutectic valley calculated with TCFE-8 with a second order polynomial of the silicon content. This gave:

$$w_C^{eut} \approx 4.335 - 0.287 \cdot w_{Si} + 0.0037 \cdot (w_{Si})^2 \qquad \text{Eqn. 10}$$

If the same procedure is applied to the carbon content calculated with Eqn. (7), one gets:

$$w_C^{eut} \approx 4.339 - 0.291 \cdot w_{Si} + 0.0040 \cdot (w_{Si})^2 \qquad \text{Eqn. 11}$$

Equations (10) or (11) converts immediately in the corresponding expression for CE:

$$CE \approx w_C + 0.287 \cdot w_{Si} - 0.0037 \cdot (w_{Si})^2 \qquad \text{Eqn. 12}$$

$$CE \approx w_C + 0.291 \cdot w_{Si} - 0.0040 \cdot (w_{Si})^2 \qquad \text{Eqn. 13}$$

The previously derived Eqn. (8) is compared with Eqn. (10) in Figure 3 where it is seen both expressions give similar values up to 3 wt% Si. Beyond this value, the quadratic form should be preferred. The same conclusion

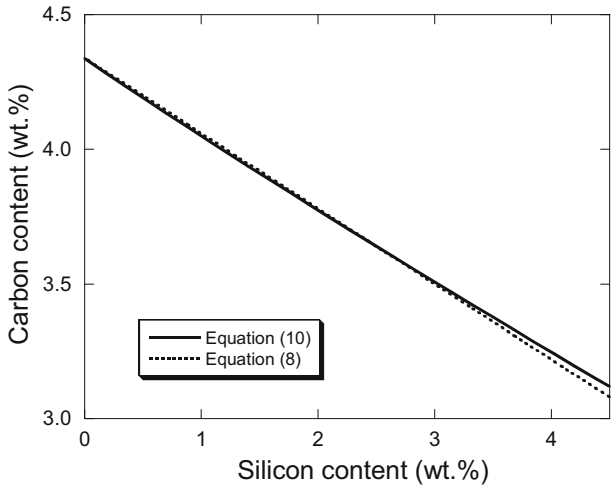

Figure 3. Change in carbon and silicon contents along the eutectic line of the stable Fe–C–Si system according to Eqns. (8) and (10).

applies to the estimate of CE, with Eqn. (9) that should be replaced by either of the two Eqns. (12) and (13) at silicon content higher than 3 wt%.

From the isopleth sections at 2, 3 and 4.5 wt% Si calculated with TCFE-8, the austenite composition was also obtained in terms of carbon and silicon contents from which the partition coefficients k_i of alloying element i (i = C, Si) between austenite and liquid could be calculated. The same procedure as before was then applied, consisting in finding an appropriate polynomial for k_C and k_{Si} for each silicon content, and then expressing the constants in these polynomial as function of the silicon content. The partition coefficients could finally be expressed as:

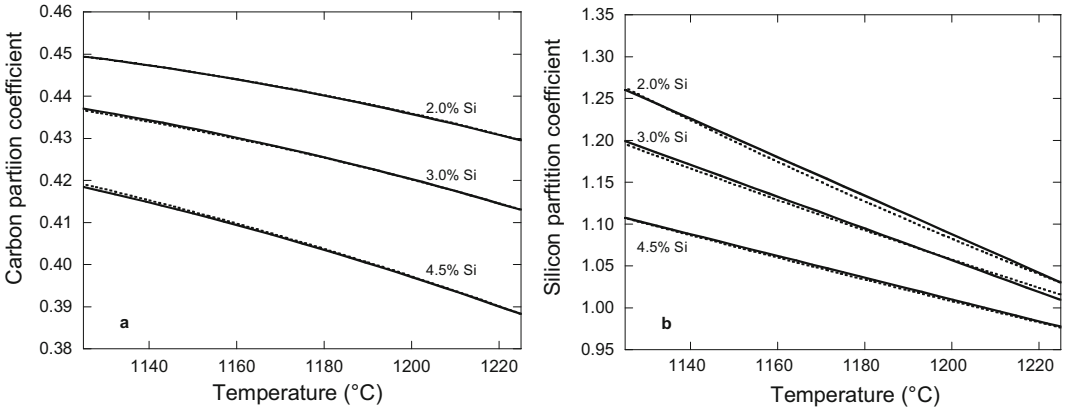

Figure 4. Partition coefficients for carbon (a) and silicon (b) according to Eqns. (14) and (15), respectively, shown in solid lines and compared with ThermoCalc calculations in dashed lines.

$$k_C = 0.4625 - 0.0165 \cdot w_{Si} + \left(1.86 \cdot 10^{-4} + 4.08 \cdot 10^{-5} \cdot w_{Si}\right) \cdot \Delta T - 6.8 \cdot 10^{-7} \cdot \Delta T^2$$

Eqn. 14

$$k_{Si} = 1.0729 - 0.0212 \cdot w_{Si} + \left(0.0031 - 4.0 \cdot 10^{-4} \cdot w_{Si}\right) \cdot \Delta T$$

Eqn. 15

in which ΔT=1225-T has been introduced to give an appropriate reference value to the constant in each equation.

Figure 4a compares the partition coefficient of carbon as calculated with Eqn. (14) (solid lines) to that coming from TCFE8 (dotted lines), and Figure 4b the same for silicon with Eqn. (15). It is seen that the agreement is perfect for carbon and excellent for silicon, allowing accurate prediction of the evolution of the austenite composition during solidification.

Effect of Additional Elements, Cu, Mn, Cr and P

For each of the selected additional elements, a number of calculations of the austenite liquidus were successively performed similarly to the previous section. Copper was added at a level of 1 wt% and it was soon realized that it does not show a simple linear effect, with both T_0^γ and the m_C^γ terms depending on the silicon content. It was also necessary to include the Fe–C isopleth at 1 wt% Cu to properly describe the liquidus behavior at low silicon contents. It was finally found that the following equations could describe the effects of silicon and copper:

$$T_0^\gamma = 1639.0 - 49.652 \cdot w_{Si} + 2.7506 \cdot (w_{Si})^2 - \left\{26.531 - 11.571 \cdot w_{Si} + 1.6962 \cdot (w_{Si})^2\right\} \cdot w_{Cu}$$

Eqn. 16

$$m_C^\gamma = -112.21 + 6.0457 \cdot w_{Si} - 0.51415 \cdot (w_{Si})^2 + \left\{5.4439 - 2.979 \cdot w_{Si} + 0.59873 \cdot (w_{Si})^2\right\} \cdot w_{Cu}$$

Eqn. 17

Figure 5a compares the austenite liquidus for 1 wt% Cu and 0, 2, 3 and 4.5 wt% Si as calculated with TCFE8 and with Eqn. (1) when the above parameters are used. There is a slight underestimation with the polynomial approach at 2 wt% Si and an overestimation at 3 wt% Si, while the agreement is excellent at 0 wt% and 4.5 wt% Si.

The effect of 0.5 wt% Mn added was investigated and found to decrease the austenite liquidus by less than 3°C with a small effect of the silicon content on this decrease. The correction term to T_0^γ could thus be expressed as: $(-5.88 + 0.12 \cdot w_{Si}) \cdot w_{Mn}$. Figure 5b compares the austenite liquidus as calculated with TCFE-8 and using Eqn. (16) with this correction included. It is seen a slight underestimation at 3 wt% Si while the curves are properly superimposed at 2 and 4.5 wt% Si.

Finally, the effects of 0.25 wt% of Cr and P were evaluated for 3 wt% Si as illustrated in Figure 6 that shows a simple shift of the liquidus that is positive for Cr and negative for P. This could be taken into account by simply adding $+ 6 \cdot w_{Cr}$ and $- 48 \cdot w_P$ to the T_0^γ term.

Considering a simple additive effect of these four additional elements, the final expression of T_0^{γ} thus is:

$$T_0^{\gamma} = 1639.0 - 49.652 \cdot w_{Si} + 2.7506 \cdot (w_{Si})^2 + (-5.88 + 0.12 \cdot w_{Si}) \cdot w_{Mn} + 6.0 \cdot w_{Cr} - 48.0 \cdot w_P - \left\{26.531 - 11.571 \cdot w_{Si} + 1.6962 \cdot (w_{Si})^2\right\} \cdot w_{Cu} \quad \text{Eqn. 18}$$

while that of m_C^{γ} is given by Eqn. (17).

For the graphite liquidus, calculations with TCFE-8 have been performed only at 3 wt% Si and are plotted in Figure 7 that evidences a simple shift to higher or lower temperature depending on the addition. Accordingly, T_L^{gra} is expressed using Eqn. (2) with m_C^{gra} unchanged and given by Eqn. (6) while T_0^{gra} is now written:

$$T_0^{gra} = -503.34 + 196.46 \cdot w_{Si} - 11.368 \cdot (w_{Si})^2 + 22.3 \cdot w_{Cu} - 6.6 \cdot w_{Mn} - 26.0 \cdot w_{Cr} + 78.4 \cdot w_P \quad \text{Eqn. 19}$$

Equations 16–19 are valid for silicon contents of 2–4.5 wt%, and carbon contents identical to those in Eqns. 1–6, i.e. a maximum of 4.5 wt% regardless of silicon content, and a minimum of 3 wt% for 2 wt% Si and 2.5 wt% for 4.5 wt% Si.

By equating the austenite and graphite liquidus expressions, one gets an updated equation for w_C^{eut}:

$$w_C^{eut} = 4.333 \cdot \frac{1 - 0.1149 \cdot w_{Si} + 0.0066 \cdot (w_{Si})^2 - 0.0228 \cdot \left[1 - 0.2370 \cdot w_{Si} + 0.0347 \cdot (w_{Si})^2\right] \cdot w_{Cu} + 0.0003 \cdot (1 + 0.1666 \cdot w_{Si}) \cdot w_{Mn} + 0.0149 \cdot w_{Cr} - 0.0590 \cdot w_P}{1 - 0.0515 \cdot w_{Si} + 0.0044 \cdot (w_{Si})^2 - 0.0110 \cdot \left[1 - 0.5472 \cdot w_{Si} + 0.1100 \cdot (w_{Si})^2\right] \cdot w_{Cu}} \quad \text{Eqn. 20}$$

This equation has been plotted on Figure 8a for the Fe–C–Si ternary system without and with each of the considered additions. Copper added at 1 wt% and phosphorus added at 0.25 wt% have nearly the same effect in shifting the eutectic line towards the Fe corner, while chromium at 0.25 wt% enlarges slightly the austenite domain. Manganese added at 0.5 wt% has practically no effect and the

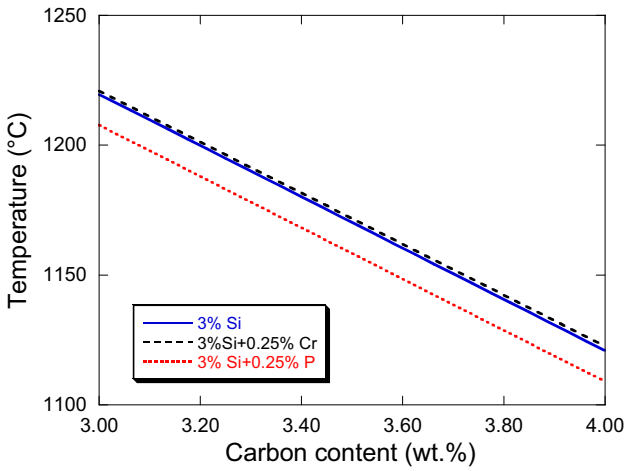

Figure 6. Effect of 0.25 wt% Cr and 0.25 wt% P on the austenite liquidus at 3 wt% Si as calculated with TCFE-8.

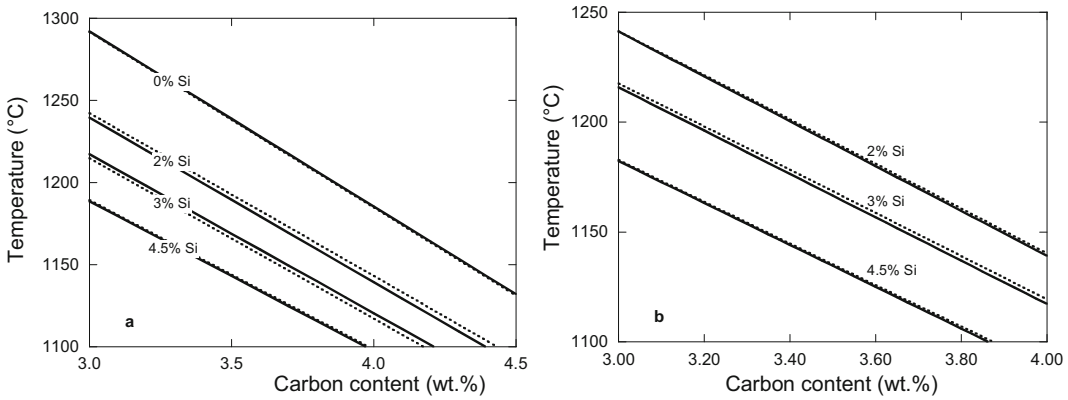

Figure 5. Austenite liquidus at various Si contents as calculated with TCFE8 (dotted lines) and with the polynomial expressions: effect of 1 wt% Cu (a) and of 0.5 wt% Mn (b).

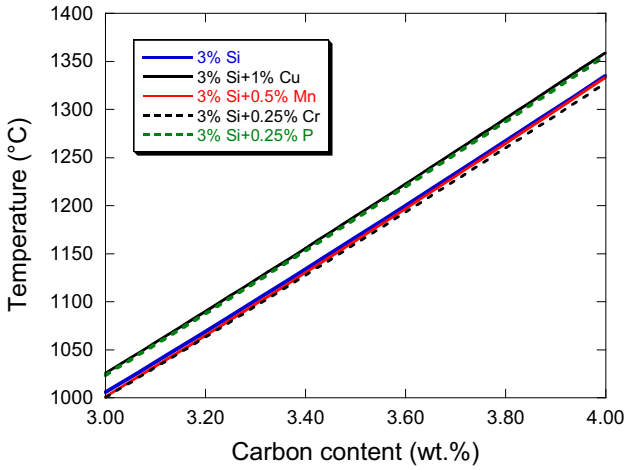

Figure 7. Effect of 1 wt% Cu, 0.5 wt% Mn, 0.25 wt% Cr and 0.25 wt% P on the graphite liquidus at 3 wt% Si. Calculations performed with TCFE-8.

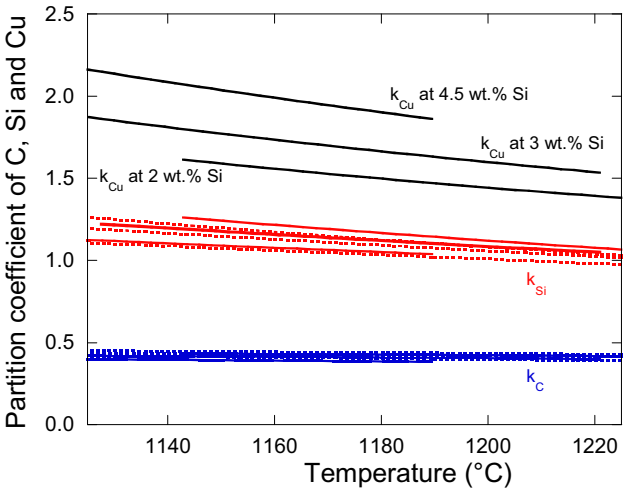

Figure 9. Partition coefficient of Cu and effect of 1 wt% Cu on the partition coefficient of carbon and silicon. Dotted lines are for alloys without Cu, solid lines for alloys with 1 wt% Cu. All calculations performed with TCFE-8.

corresponding eutectic trough is superimposed to that in the ternary Fe-C-Si system.

Analysis of the differences between the composition along the eutectic trough without addition and with each of the additions showed it varies little with the silicon content. Though it would be better to use Eqn. (20) for evaluating w_C^{eut}, an estimate of the alloying effects could be obtained in the same way as for Eqn. (11). It writes as following:

$$w_C^{eut} \approx 4.339 - 0.291 \cdot w_{Si} + 0.0040 \cdot (w_{Si})^2 - 0.05 \cdot w_{Cu} + 0.07 \cdot w_{Cr} - 0.276 \cdot w_P$$

Eqn. 21

This gives the following approximate expression for CE:

$$CE \approx w_C + 0.291 \cdot w_{Si} - 0.0040 \cdot (w_{Si})^2 + 0.05 \cdot w_{Cu} - 0.07 \cdot w_{Cr} + 0.276 \cdot w_P$$

Eqn. 22

in which manganese plays no role as expected from above.

The effect of each alloying addition on the eutectic temperature is plotted in Figure 8b that shows contrasted features because their effects on the austenite and graphite liquidus are different. The two so-called carbide promoters, Mn and Cr, lower the graphite liquidus while manganese lowers and chromium increases the austenite liquidus. In turn, manganese decreases the eutectic temperature when chromium has little effect on it. The two "graphite formers," copper and phosphorus, have a similar effect on graphite liquidus, which they increase, and on austenite liquidus, which they decrease, with phosphorus being far more effective.

The final step of analysis of individual additions was to evaluate the partition coefficients, both of the extra additions but also of carbon and silicon to check for any cross-effect. Figure 9 shows the effect of 1 wt% Cu on the partition coefficient of carbon and silicon, with dotted and

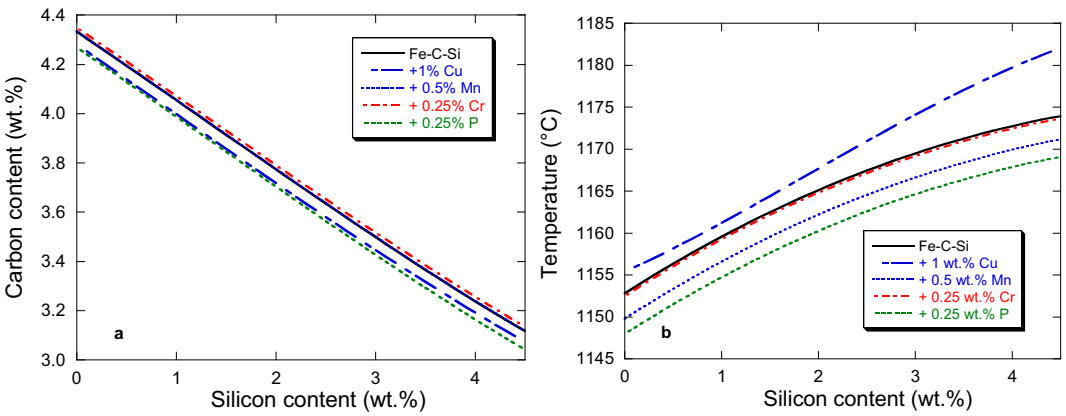

Figure 8. Effect of alloying addition on: (a) the eutectic composition according to Eqn. (20). (b) The eutectic temperature.

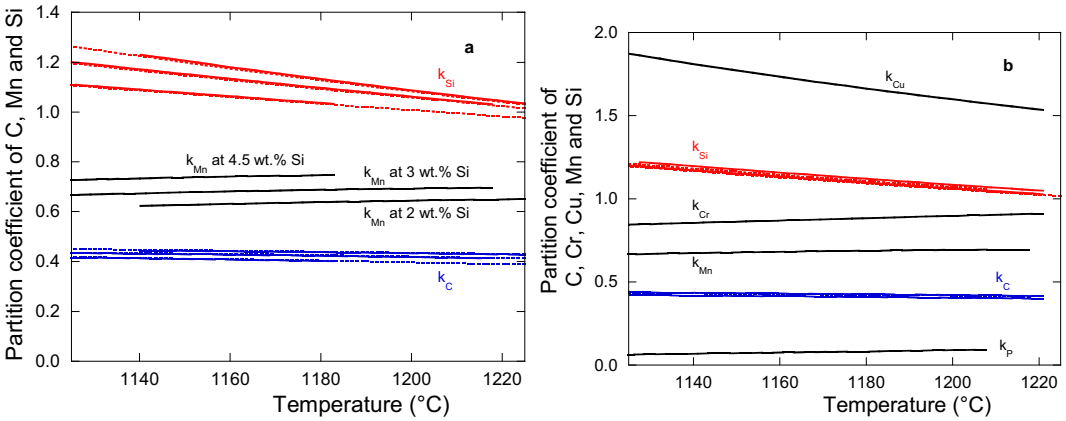

Figure 10. (a) Partition coefficient of Mn and effect of 0.5 wt% Mn on the partition coefficient of C and Si. Dotted lines for calculations without Mn and solid lines with Mn. (b) Solid lines show the partition coefficient of Cu (1. wt%), Mn (0.5 wt%), Cr (0.25 wt%) and P (0.25 wt%) at 3 wt% Si. The partition coefficient of carbon and silicon without (dotted lines) and with (solid lines) single additions are also plotted. All calculations carried out with TCFE-8.

solid lines representing TCFE-8 calculations without and with addition of copper, respectively. It is seen reasonable to consider that addition of copper has little effect on these partition coefficients. The graph also shows that silicon and temperature have a significant effect on the partition coefficient of copper that could be described by:

$$k_{Cu} = 1.1336 + 0.12145 \cdot w_{Si} + \left(0.000963 + 8.7 \cdot 10^{-4} \cdot w_{Si}\right) \cdot \Delta T \qquad \text{Eqn. 23}$$

Figure 10a shows similarly the effect of 0.5 wt% Mn and again it is noticed very little effect of this addition to the partition coefficient of carbon and silicon. The effect of silicon and temperature on the partition coefficient of manganese could be described as:

$$k_{Mn} = 0.557 + 0.047 \cdot w_{Si} - \left[0.00026 - 9.0 \cdot 10^{-6} \cdot (w_{Si})^2\right] \cdot \Delta T \qquad \text{Eqn. 24}$$

Finally, Figure 10b compares the partition coefficient of all elements, C, Si, Cu, Mn, Cr and P as function of temperature for 3 wt% Si. Owing to the low level considered for Cr and P, it is not expected an effect of the silicon content on their partition coefficients that were then described as:

$$k_{Cr} = 0.9146 - 0.0007 \cdot \Delta T \qquad \text{Eqn. 25}$$

$$k_P = 0.0982 - 0.00035 \cdot \Delta T \qquad \text{Eqn. 26}$$

Discussion

Thermodynamic software such as Thermocalc, used in this work, calculates the minimum of the Gibbs energy to determine which phases may be present for a given set of conditions, namely pressure, temperature and composition. The description of the phases follows various models depending on the type of phase, solid, liquid, compound,

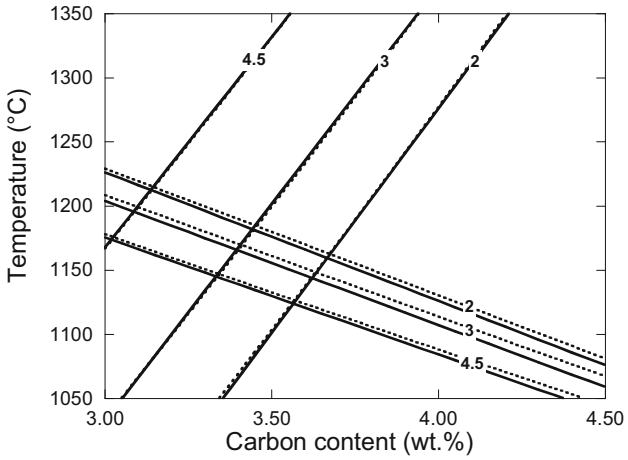

Figure 11. Comparison of austenite and graphite liquidus calculated with TCFE-8 (dotted lines) and with the polynomial description (solid lines) for alloys containing 1 wt% Cu, 0.5 wt% Mn, 0.25 wt% Cr and 0.25 wt% P, and 2, 3 and 4.5 wt% silicon (as indicated). The austenite liquidus decreases with carbon content, while the graphite liquidus raises with it.

etc., that write as polynomials of composition and temperature, and possibly also of pressure, which are stored in databanks such as TCFE-8. While the Gibbs energy calculations are perfectly achieved, it is clear that the outputs of the calculations rely on the accuracy of the databanks. It is here considered that the ternary Fe-C-Si system is effectively properly described by the TCFE-8 databank. As a matter of fact, the early assessment[21] was intended to provide a good description of the eutectic valley and the modifications proposed by Miettinen[23] did maintain the good fit between calculated and experimental eutectic temperature as shown in Figure 2b. It is not sure that such a good description of the eutectic valley was achieved in the more recent reassessment by Wei-sen Zheng et al.[24] that

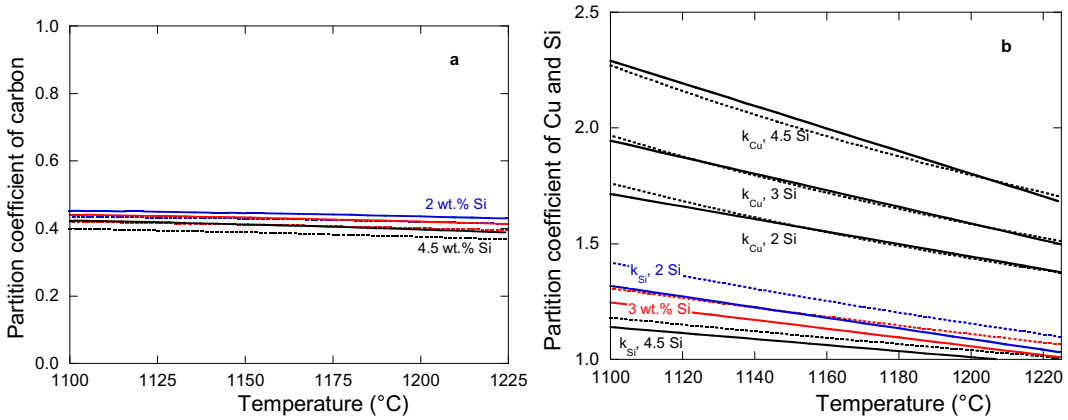

Figure 12. Comparison of the partition coefficient (carbon in (a) and copper and silicon in (b)) calculated with TCFE-8 (dotted lines) and with the polynomial description (solid lines) for alloys containing 1 wt% Cu, 0.5 wt% Mn, 0.25 wt% Cr and 0.25 wt% P, and 2, 3 and 4.5 wt% silicon (as indicated).

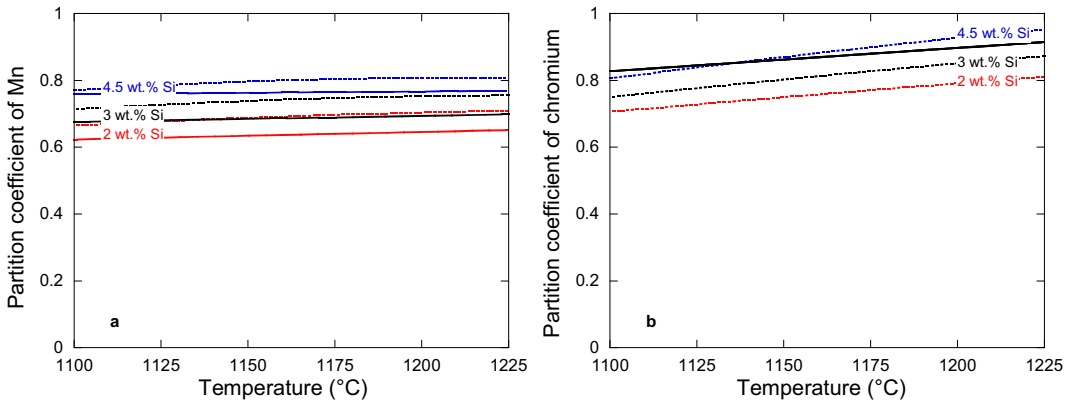

Figure 13. Comparison of the partition coefficient (manganese in (a) and chromium in (b)) calculated with TCFE-8 (dotted lines) and with the polynomial description (solid lines) for alloys containing 1 wt% Cu, 0.5 wt% Mn, 0.25 wt% Cr and 0.25 wt% P, and 2, 3 and 4.5 wt% silicon (as indicated).

focused on low carbon steels, and it was found safe to rely on TCFE-8 for the present work.

A further assumption in the present approach is that the four alloying elements were added at low enough levels to ensure a fair description in the eutectic range up to 4.5 wt% Si in the Fe–C–Si–Cu–Cr–Mn–P system by simply adding their effects in the polynomial description. To check this, the predictions made with the polynomials described in the previous section were compared to TCFE-8 calculations for alloys containing 1 wt% Cu, 0.5 wt% Mn, 0.25 wt% Cr and 0.25 wt% P. This comparison is illustrated in Figures 11, 12, 13 for 2, 3 and 4.5 wt% silicon.

Figure 11 shows that the austenite and graphite liquidus are properly described, with a difference of at most 5°C for the eutectic temperature. This discrepancy is mostly due to the high copper content that was considered, and would be less than 1.5 °C at the more usual content of 0.25 wt% Cu.

Figure 12 presents the partition coefficient for carbon (Figure 12a) and copper and silicon (Figure 12b) in the temperature range of interest and for the three silicon contents. In Figure 12a, it is seen that the polynomial description slightly overestimates the carbon partition coefficient, but that the change with silicon content is correctly evaluated. Figure 12b demonstrates that the copper partition coefficient is well reproduced, while the silicon partition coefficient is slightly underestimated, though again the effect of silicon content is well accounted for. Figure 13a presents the partition coefficient for manganese that appears to be slightly underestimated with the polynomial description, but with an effect of silicon content that is properly described. In Figure 13b, there is only one curve for the polynomial description of the chromium partition coefficient as Eqn. (25) did not include any effect of silicon. Although the TCFE-8 calculations show a downwards shift at decreasing silicon content, the description with Eqn. (25) will certainly be sufficient to properly predict chromium microsegregation. Finally, the

phosphorus partition coefficient was found to be perfectly reproduced with Eqn. (26) for the three silicon contents that have been considered and was not shown again.

Kagawa and Okamoto[25] have calculated the partition coefficients in several ternary Fe–C–X systems based on thermodynamic interaction parameters determined at high temperatures, and they extrapolated their calculations down to 1150 °C for C, Cr, Mn, Si and Ni. Their values for C, Mn and Si are quite similar to those reported in the present work, while for Cr they are lower at about 0.5 at 1150°C. Also, Kagawa et al. calculated a partition coefficient for Cu of 1.57 that is lower than the present values, while Figure 20 of Parameswaran et al.[26] suggests a partition coefficient of about 2 for copper in the Fe–C–Cu system at 1155 °C that is more in agreement with the present description.

Conclusion

Knowledge of the equilibrium stable phase diagram is a prerequisite for modelling solidification of silicon cast irons, from which off equilibrium departure can be predicted. This includes nucleation and growth undercooling that have been described for austenite[14,27,28] as well as for spheroidal graphite.[3] An important feature of the present work was to consider also the partition coefficients of the most usual alloying elements found in cast irons (copper, chromium, manganese and phosphorus), the knowledge of which will allow to predict build-up of microsegregation. According to phase field modeling, redistribution of substitutional solutes such as silicon and the above listed alloying elements can effectively be described using Scheil's model[29] as was assumed in previous works.[30,31] In summary, the present paper provides the practical tool necessary for extending these simulation approaches to high silicon cast irons.

Funding

Open access funding provided by Institut National Polytechnique de Toulouse.

REFERENCES

1. M. Castro, M. Herrera, M.M. Cisneros, G. Lesoult, J. Lacaze, Simulation of thermal analysis applied to the description of the solidification of hypereutectic SG cast irons. Int. J. Cast Met. Res. **11**, 369–374 (1999)
2. A. Regordosa, U. de la Torre, J. Sertucha, J. Lacaze, Quantitative analysis of the effect of inoculation and magnesium content on compacted graphite irons—experimental approach. J. Mater. Process. Technol. **9**, 11332–11343 (2020). https://doi.org/10.1016/j.jmrt.2020.08.008
3. M.J. Castro-Román, J. Lacaze, A. Regordosa, J. Sertucha, R. del Campo-Castro, Revisiting thermal analysis of hypereutectic spheroidal graphite cast irons. Metall. Mater. Trans. **51A**, 6373–6386 (2020). https://doi.org/10.1007/s11661-020-06005-7
4. A. Regordosa, J. Sertucha, J.R. Olaizola, J. Lacaze, When is a cast iron eutectic? Int. J. Metalcast. **16**, 119–131 (2022). https://doi.org/10.1007/s40962-021-00587-7
5. A. Regordosa, J. Lacaze, J. Sertucha, M.J. Castro-Roman, U. de la Torre, O. Dezellus, Is thermal analysis able to provide carbon and silicon contents of cast irons? Int. J. Metalcast. **17**, 592–603 (2023). https://doi.org/10.1007/s40962-022-00799-5
6. J. Lacaze, Kinetic effects on the austenite carbon equivalent and eutectic carbon equivalent of silicon cast irons. Int. J. Metalcast. **17**, 2062–2071 (2023). https://doi.org/10.1007/s40962-022-00919-1
7. M.D. Chaudhari, R.W. Heine, C.R. Loper, Principles involved in the use of cooling curves in ductile iron process control. AFS Cast Met. Res. J. **11**, 52–60 (1975)
8. L. Backerud, K. Nilsson, M. Steen, Study of nucleation and growth of graphite in magnesium-treated cast iron by means of thermal analysis. In: The metallurgy of cast Iron. GeorgiPub. Co.; 1975. p. 625–37.
9. R.W. Heine, Liquidus and eutectic temperatures and solidification of white cast irons. AFS Trans. **85**, 537 (1977)
10. A. Alagarsamy, F.W. Jacobs, G.R. Strong, R.W. Heine, Carbon equivalent vs. austenite liquidus: What is the correct relationship for cast irons? AFS Trans. **92**, 871 (1984)
11. R.W. Heine, The Fe-C-Si solidification diagram for cast irons. AFS Trans. **94**, 391 (1986)

12. W. Menk, M.O. Speidel, and R. Döpp. Giesserei-forschung. **44**, 66–79 (1992)
13. R.W. Heine, Austenite liquidus, carbide eutectic and undercooling in process control of ductile base iron. AFS Trans. **103**, 199 (1995)
14. F. Mampaey, Application of austenite dendrite growth model to analyse liquidus temperature measurements in cups. AFS Trans. **106**, 461–467 (1998)
15. S. Rodriguez, M. Castro, M. Herrera, J. Mendez, J.I. Escalante, C. Gonzalez, Thermal analysis of compacted graphite cast irons containing various levels of Mg and S. Int. J. Cast Met. Res. **11**, 381–386 (1999)
16. A. Dioszegi, V.L. Diaconu, V. Fourlakidis, Prediction of volume fraction of primary austenite at solidification of lamellar graphite cast iron using thermal analyses. J. Therm. Anal. Calorim. **124**, 215–225 (2016)
17. V. Anjos, R. Deike, C.S. Ribeiro, The use of thermal analysis to predict the dendritic coherency point on nodular cast iron melts. Cienca Tecnol. Mater. **29**, e27–e33 (2017)
18. D.M. Stefanescu, Analysis of the rationale and accuracy of the use of carbon equivalent and thermal analysis in the quality control of cast iron. Int. J. Metalcast. **16**, 1057–1078 (2022). https://doi.org/10.1007/s40962-021-00685-6
19. Thermo-Calc Software database TCFE version 8. https://thermocalc.com/products/databases/steel-and-fe-alloys/
20. V.E. Bazhenov, M.V. Pikunov, Determining the carbon equivalent of cast iron by the Thermo_Calc program. Steel Transl. **41**, 896–899 (2011)
21. J. Lacaze, B. Sundman, An assessment of the Fe-C-Si system. Metall. Trans. **22A**, 2211–2223 (1991)
22. J. Lacaze, J. Sertucha, M.J. Castro-Román, A contemporary monograph on silicon cast irons microstructure—from atom scale to casting (2024). https://hal.science/hal-04447564
23. J. Miettinen, Reassessed thermodynamic solution phase data for ternary Fe-Si-C system. Calphad **22**, 231–256 (1998)
24. W.-S. Zheng, Lu. Xiao-gang, Y.-L. He, L. Li, Thermodynamic modeling of Fe-C-Mn-Si alloys. J. Iron. Steel Res. Int. **24**, 190–197 (2017)
25. A. Kagawa, T. Okamoto, Partition of alloying elements on eutectic solidification of cast iron, in The physical metallurgy of cast iron. Mat. Res. Soc. Symp. **34**, 201–210 (1985)
26. K. Parameswaran, K. Metz, A. Morris, Phase equilibria for iron-rich Fe-Cu-C alloys: 1500 to 950°C. Metall. Trans. A **10A**, 1929–1939 (1979)
27. N. Siredey, J. Lacaze, Growth conditions at the solidification front of multicomponent alloys. Scr. Metall. Mater. **29**, 759–764 (1993)
28. E. Fras, W. Kapturkiewicz, A.A. Burbielko, H.F. Lopez, Numerical simulation and Fourier thermal analysis of solidification kinetics in high-carbon Fe-C alloys. Metall. Mater. Trans. B **28B**, 115–123 (1997)
29. J. Eiken, E. Subasic, J. Lacaze, 3D phase-field computations of microsegregation in nodular cast iron compared to experimental data and CalPhad-based Scheil-prediction. Materialia **9**, 100538 (2020). https://doi.org/10.1016/j.mtla.2019.100538
30. J. Lacaze, Solidification of spheroidal graphite cast irons. Part III: microsegregation related effects. Acta Mater. **47**, 3779–3792 (1999)
31. C. Selig, J. Lacaze, Study of microsegregation buildup during solidification of spheroidal graphite cast iron. Metall. Mater. Trans. B **31B**, 827–836 (2000)